Holes with very acute angles: a new paradigm of extraordinary optical transmission through strongly localized modes

Sergio G. Rodrigo,[1,*] O. Mahboub,[2] A. Degiron,[3] Cyriaque Genet,[2] F. J. García-Vidal,[4] L. Martín-Moreno,[1] and Thomas W. Ebbesen[2]

[1] *Instituto de Ciencia de Materiales de Aragón and Departamento de Física de la Materia Condensada, CSIC-Universidad de Zaragoza, E-50009, Zaragoza, Spain*
[2] *ISIS, Université de Strasbourg and CNRS, 67000 Strasbourg, France*
[3] *IEF, Université Paris-Sud and CNRS, 91405 Orsay, France*
[4] *Departamento de Física Teórica de la Materia Condensada, Universidad Autónoma de Madrid, Madrid 28049, Spain*

**sergut@unizar.es*

Abstract: It is shown that submicrometer holes with very acute angles present extraordinary optical transmission peaks associated to strongly localized modes. The positions of these peaks are: (i) strongly redshifted with respect to the peak position that could be expected if the considered hole were in a film made of perfect electric conductor, (ii) independent on the angle of incidence for a large range of angles and (iii) strongly dependent on the direction of the incident electric field. In addition, it is demonstrated that these properties are linked to the mechanisms leading to the existence of channel-plasmon-polaritons.

OCIS codes: (050.6624) Subwavelength structures; (050.1220) Apertures; (240.6680) Surface plasmons; (050.2770) Gratings; (050.1960) Diffraction theory.

References and links

1. T. W. Ebbesen, H. J. Lezec, H. F. Ghaemi, T. Thio, and P. A. Wolff, "Extraordinary optical transmission through sub-wavelength hole arrays," Nature **391**, 667–669 (1998).
2. F. J. Garcia-Vidal, L. Martin-Moreno, T. W. Ebbesen, and L. Kuipers, "Light passing through subwavelength apertures," Rev. Mod. Phys. **82**, 729–787 (2010).
3. L. Martin-Moreno, F. J. Garcia-Vidal, H. J. Lezec, K. M. Pellerin, T. Thio, J. B. Pendry, and T. W. Ebbesen, "Theory of extraordinary optical transmission through subwavelength hole arrays," Phys. Rev. Lett. **86**, 1114–1117 (2001).
4. F. J. García de Abajo and J. J. Sáenz, "Electromagnetic surface modes in structured perfect-conductor surfaces," Phys. Rev. Lett. **95**, 233901 (2005).
5. K. L. van der Molen, F. B. Segerink, N. F. van Hulst, and L. Kuipers, "Influence of hole size on the extraordinary transmission through subwavelength hole arrays," Appl. Phys. Lett. **85**, 4316–4318 (2004).
6. A. Degiron and T. W. Ebbesen, "The role of localized surface plasmon modes in the enhanced transmission of periodic subwavelength apertures," J. Opt. A, Pure Appl. Opt. **7**, S90–S96 (2005).
7. A. Degiron, H. J. Lezec, N. Yamamoto, and T. W. Ebbesen, "Optical transmission properties of a single subwavelength aperture in a real metal," Opt. Commun. **239**, 61–66 (2004).
8. J. W. Lee, M. A. Seo, D. H. Kang, K. S. Khim, S. C. Jeoung, and D. S. Kim, "Terahertz electromagnetic wave transmission through random arrays of single rectangular holes and slits in thin metallic sheets," Phys. Rev. Lett. **99**, 137401 (2007).
9. F. J. Garcia-Vidal, E. Moreno, J. A. Porto, and L. Martin-Moreno, "Transmission of light through a single rectangular hole," Phys. Rev. Lett. **95**, 1–4 (2005).

#132559 - $15.00 USD Received 2 Aug 2010; revised 9 Sep 2010; accepted 10 Sep 2010; published 27 Oct 2010

10. F. I. Baida and D. Van Labeke, "Three-dimensional structures for enhanced transmission through a metallic film: Annular aperture arrays," Phys. Rev. B **67**, 155314 (2003).
11. S. M. Orbons and A. Roberts, "Resonance and extraordinary transmission in annular aperture arrays," Opt. Express **14**, 12623–12628 (2006).
12. J. H. Kim and P. J. Moyer, "Transmission characteristics of metallic equilateral triangular nanohole arrays," Appl. Phys. Lett. **89**, 121106 (2006).
13. J. H. Kim and P. J. Moyer, "Thickness effects on the optical transmission characteristics of small hole arrays on thin gold films." Opt. Express **14**, 6595 (2006).
14. E. D. Palik, *Handbook of Optical Constants of Solids* (Academic Press, 1985).
15. A. Taflove and S. Hagness, *Computational Electrodynamics: The Finite-Difference Time-Domain Method* (Artech House, Boston, 2000).
16. S. G. Rodrigo, F. J. Garcia-Vidal, and L. Martin-Moreno, "Influence of material properties on extraordinary optical transmission through hole arrays," Phys. Rev. B **77**, 075401 (2008).
17. W. L. Barnes, W. A. Murray, J. Dintinger, E. Devaux, and T. W. Ebbesen, "Surface plasmon polaritons and their role in the enhanced transmission of light through periodic arrays of subwavelength holes in a metal film," Phys. Rev. Lett. **92**, 107401 (2004).
18. S. I. Bozhevolnyi, V. S. Volkov, E. Devaux, J. Y. Laluet, and T. W. Ebbesen, "Channel plasmon subwavelength waveguide components including interferometers and ring resonators," Nature **440**, 508 (2006).
19. E. Moreno, F. J. Garcia-Vidal, S. G. Rodrigo, L. Martin-Moreno, and S. I. Bozhevolnyi, "Channel plasmon-polaritons: modal shape, dispersion, and losses," Opt. Lett. **31**, 3447–3449 (2006).

1. Introduction

The discovery of the Extraordinary Optical Transmission (EOT) in arrays of subwavelength holes, drilled in optically thick metal films [1] has attracted a great deal of attention, due both to its fundamental character and potential applications [2]. In its original form, the transmission resonances occur at wavelengths larger than the cutoff of the holes. The transmission is then mediated by the aid of electromagnetic (EM) surface modes supported by the holey surfaces [3, 4]. Experiments on the dependence of EOT with hole shape revealed, both in arrays [5, 6] and in isolated holes [7, 8], the existence of another type of transmission resonances, which arise from EM modes localized close to the hole. These resonances can be understood as a Fabry-Perot mode inside the hole which, for a symmetric dielectric environment, appear spectrally close to the condition of vanishing propagation constant [9], i.e., close to the cutoff wavelength of the hole (λ_c). While the resonances due to surface modes depend on the parallel wavevector involved, and therefore on the angle of incidence, the ones due to localized modes are largely angle independent, provided that the resonant wavelength is much larger than both the size of the hole and the lattice constant. We can thus define "large cutoff holes" (LCH) as those with $\lambda_c \gg 2\sqrt{A}$, A being the aperture area, i.e., holes with a cutoff wavelength much larger than that of a square hole in vacuum with the same area. Examples of LCH are narrow rectangular holes, annular holes [10, 11], and any hole filled with a material with dielectric constant much larger than those in the transmission and reflection regions.

We show here, both experimentally and theoretically, that submicrometer holes with very acute angles belong to this "large cut-off" category in the optical regime. For that, we consider the exemplary system of a square lattice of isosceles triangular holes (with an acutest angle of $\sim 43^0$) on a silver film. We show that the transmission resonances are nearly dispersionless, although they are strongly dependent on the direction of the incident electric field. We also demonstrate that these properties are linked to the existence of channel-plasmon-polaritons (CPPs), which reinforces their plasmonic origin. The optical transmission through arrays of triangular holes have been considered before, but only for the *equilateral* shape [12, 13]. In this case, although the EOT peaks showed some unexpected shifts, the angles were not acute enough to clearly show the underlying mechanisms, nor to manifest the independence with angle of incidence.

#132559 - $15.00 USD Received 2 Aug 2010; revised 9 Sep 2010; accepted 10 Sep 2010; published 27 Oct 2010

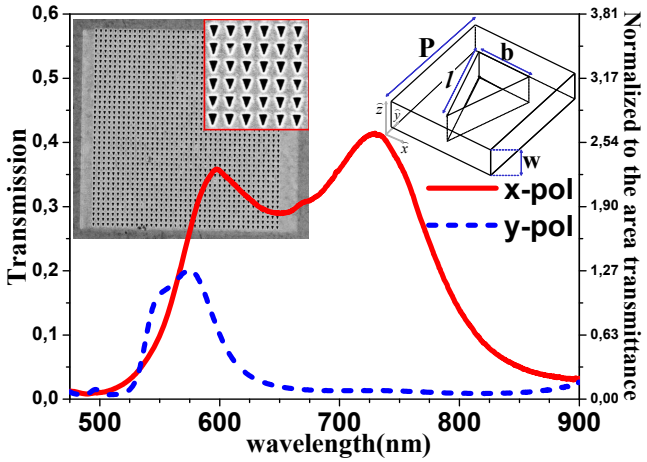

Fig. 1. Experimental zero-order transmittance at normal incidence through a square array of isosceles triangular holes perforated on a free-standing silver metal slab ($P = 450$nm, $w = 320$nm, $l = 305$nm and $b = 225$nm, with the geometry defined in the inset at the right). The incident electric field points either along the x-direction (solid red curve) or y-direction (dashed blue curve). An SEM image of the experimental sample is shown in the inset at the left.

2. Experimental and theoretical results

In the experiments, the lattice parameter was fixed at $P = 450$nm and the film thickness $w = 320$nm. The triangles were characterized by a base $b = 225$nm, aligned along one of the axis of the array, and legs $l = 305$nm (see Fig. 1). The array was fabricated in an Ag film suspended in air. In this case, we expect surface modes to induce transmission peaks slightly red-shifted (by typically a few tens of nm) with respect to corresponding deep minima, which, in optically thick films, appear at the condition of grating coupling to the Surface Plasmon Polariton (SPP) of each of the flat interfaces. Using the dielectric constant for silver [14], the transmittance minimum is expected to appear at $\lambda_{min} \approx 489$nm, which is itself slightly red-shifted from the reference wavelength for surface effects (or Rayleigh wavelength) $\lambda_R = P = 450$nm. The array was illuminated by a collimated white light source and zero-order transmission spectra were measured using an inverted microscope coupled to a visible-range spectrometer. The white source being unpolarized, the direction of the incident electric field was chosen using a linear polarizer. Figure 1 renders the measurements for normal incidence and for the electric field pointing either along the base of the triangles (x-polarization, solid red curve) or perpendicular to it (y-polarization, dashed blue curve). The experimental spectra display peaks of high transmittance at wavelength much larger than those expected if surface modes were involved. This occurs for both polarizations, but it is more noticeable for x-polarization. Noticeably, the normalized to the area transmittance (right axis of Fig. 1) is greater than 1 for both polarizations.

To understand these results we have computed the optical response of the considered system using the Finite-Difference-Time-Domain (FDTD) method [15, 16]. Figure 2(a) shows the computed transmission and reflection spectra for both $x-$ and $y-$ polarizations. These data present the expected transmittance minimum at λ_{min} and, as in the experiments, transmission peaks strongly redshifted from it. The overall shape of the computed transmission spectra is in good agreement with the experimental one. The computed transmission resonances appear at slightly larger wavelengths than the corresponding experimental ones, which we associate to

#132559 - $15.00 USD Received 2 Aug 2010; revised 9 Sep 2010; accepted 10 Sep 2010; published 27 Oct 2010

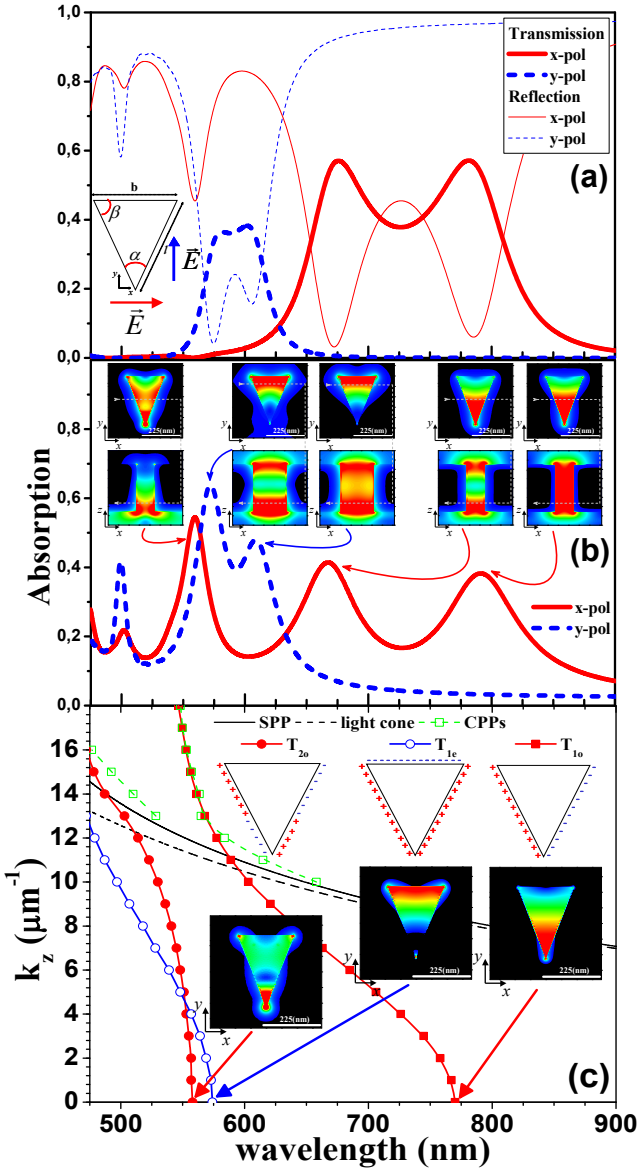

Fig. 2. (a) Calculated zero-order transmission and reflection spectra (same parameters as in Fig.1), at normal incidence, with the field pointing along the x or y axis (See label). Panel (b) shows the absorption spectra, and the electric field amplitude $|E|$ maps, at chosen wavelengths and the cross sections indicated by dashed lines. Panel (c) renders the dispersion relation for TWG modes, together with their $|E|$ maps at cutoff and the sketch of their associated charge distribution. This panel also shows the dispersion relations for (i) the two lowest CPP modes of a triangular groove carved in silver (empty square symbols), (ii) SPPs of a flat silver surface (continuous black line) and (iii) the light cone (dashed line).

the precise shape of the corners. Calculations (not shown here) for the same system but with rounded-off triangular corners present a better match to the experimental results. Nevertheless,

#132559 - $15.00 USD Received 2 Aug 2010; revised 9 Sep 2010; accepted 10 Sep 2010; published 27 Oct 2010

all calculations in this paper will be for the nominal triangular shape, in order to avoid using any fitting parameter. As Fig. 2(a) shows, some resonant features in the optical response appear more prominently in transmission, while others do in reflection. To gain insight on the main channels involved in the transmission mechanism, it is convenient to have access to the absorption spectra [17]. This magnitude is difficult to measure as, in the inherently finite real system, it requires the angular integration of both transmitted and reflected signals, but is readily accessible to the FDTD calculations. For both polarizations, the computed absorption spectra (rendered in Fig. 2(b)) show a small peak at 500nm, slightly redshifted with respect to λ_{min}. Its spectral position, and the fact that it appears for both polarizations, signals that it is due to the excitation of surface modes in the corrugated film. Additionally, for $\lambda > 525$nm the absorption spectra show three prominent peaks for $x-$polarization and two for $y-$polarization. For each peak, Fig. 2(b) renders the time-averaged modulus of the electric field, $|E|$, in both the cross section of the holes (top panels) and the perpendicular plane (bottom panels) indicated by the white dashed lines. Note the incoming light propagates upwards (along positive z direction).

The physical origin of these absorption resonances is revealed by the study of the EM modes in the isolated waveguide, with triangular cross section and translational symmetry in the $z-$direction (TWG). We term the angles of the isosceles triangle as α (the dissimilar one) and β (the two equal ones). The TWG modes are labelled as $T_{n\sigma}$, where σ refers to the parity of the charge distribution at the rim of the triangular cross section with respect to the bisector of the base ($\sigma = e, o$ for even and odd parity, respectively) and, for each parity, n numbers the modes in increasing order of frequency. Figure 2(c) shows the dispersion relation of the T_{1e}, T_{1o} and T_{2o} modes, in the form of wavevector along the longitudinal direction of the waveguide (k_z) as a function of wavelength. The inset shows schematically the charge distributions associated to these modes. Notice that, in general, the charge distribution has odd parity with respect to the bisector of the angle that mainly sustains the mode. Figure 2(c) also shows $|E|$ maps in a cross section of the isolated waveguide, at the cutoff wavelength of each mode. The comparison of these field patterns, with those in the hole array depicted in Fig. 2(b), clearly relates each absorption peak to the excitation of a TWG mode. The in-plane electric field has even symmetry in all these modes and, therefore, can couple to incident radiation at normal incidence. As can be seen in the field maps, the T_{1o} and T_{2o} modes have an $E-$field concentrated close to the α angle, whereas for the T_{1e} mode the field is concentrated close to the β angles.

Both the spectral position of the resonances and the field pattern along the hole indicate that the marked peaks originate from Fabry-Perot (FP) resonances inside the holes, satisfying $2k_z w + 2\Phi_R = 2m\pi$, where m is an integer and Φ_R is the phase picked up by the waveguide mode by reflection at each of the openings. Away from the condition of excitation of SPPs, where Φ_R changes rapidly, Φ_R can be expected to satisfy $2\Phi_R \approx 2\pi$ due to the strong impedance mismatch between the fields inside and outside the holes. Therefore, for $x-$polarization, we can assign the absorption peaks appearing at 790nm and 668nm to the $m = 0$ and $m = 1$ FP resonances of the T_{1o} TWG mode, respectively, and the absorption peak at 560nm to the $m = 0$ FP resonance of the T_{2o} mode. Notice that the field pattern at resonance has a much stronger effect on the transmission than on the absorption: the transmission resonances arising from T_{1o} modes are much stronger that the one originating from the T_{2o} mode, while all absorption peaks have similar heights and widths. For $y-$polarization, the field patterns reveal that the absorption peaks at ≈ 608nm and ≈ 572nm are due to the excitation of the T_{1e} TWG mode ($m = 0$ and $m = 1$ FP-like resonances, respectively).

The most striking feature of the array of triangular holes is the existence of "cut-off" transmission resonances at wavelengths much larger than what could naively be expected from the dimensions of the structure. To put this into perspective, the cutoff wavelength of a circular waveguide in silver, with the same area as the triangle considered, is 498.5nm, and it would be

#132559 - $15.00 USD Received 2 Aug 2010; revised 9 Sep 2010; accepted 10 Sep 2010; published 27 Oct 2010

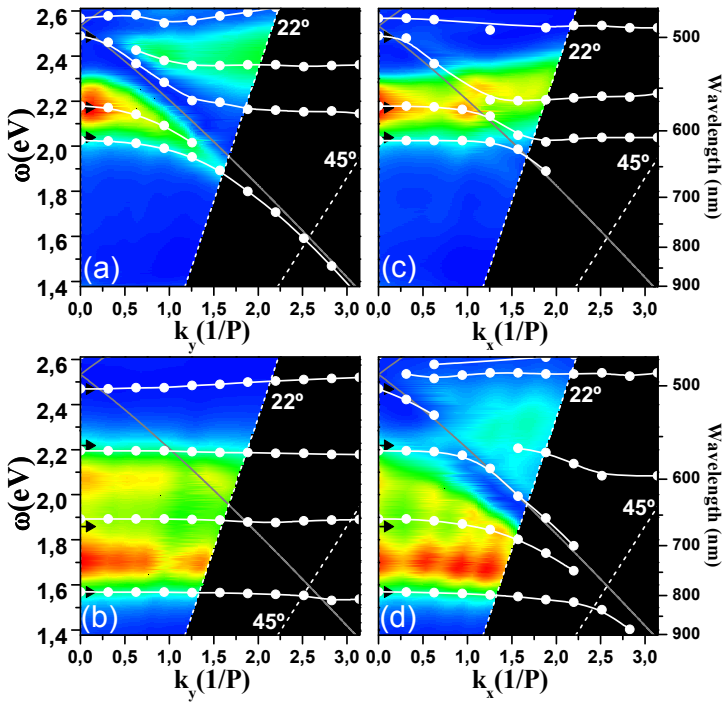

Fig. 3. Color maps: Measured transmittance as a function of both frequency and parallel momentum of the incident light, for the system considered in Fig. 1. The different panels are for different orientations and tilt angles of the incident electric field: (a) $y-$pol, tilt around the $x-$axis, (b)$x-$pol, tilt around the $x-$axis, (c) $y-$pol, tilt around the $y-$axis and (d) $x-$pol, tilt around the $y-$axis. Circular symbols depict the corresponding FDTD band structure calculations for EM bound leaky modes of the array of triangular holes in a silver film. In this case, the initial E-field points either along the x-direction (panels (b) and (d)) or along the y direction (panels (a) and (c)). The arrows mark the spectral positions of the absorption peaks at normal incidence for each polarization (see Fig. 2(b)). The SPP dispersion relation is shown by the grey line.

485nm if the considered triangular waveguide were surrounded by a perfect electrical conductor ($\varepsilon_M = -\infty$). The physical origin of the large redshift of the cutoff in TWGs in the optical regime is the same that gives rise to the strong field confinement and large cutoff wavelengths in CPPs [18, 19]. In a nutshell, this effect can be traced back to the increase in the propagation constant of a waveguide composed of two parallel metal plates, when the distance between them is decreased, which can be cast into an effective frequency-dependent dielectric constant. In an effective medium approach, the channel is considered as filled by a dielectric whose refractive index is larger at the apex (where the distance between the metal plates is smaller), thus concentrating the EM field there. To substantiate the similarities between modes in channel and triangular waveguides, we have computed the dispersion relations for EM modes inside a channel waveguide, defined by the same cross section as the TWG considered. The results for $k_z(\lambda)$ for the CPPs are rendered with empty square symbols in Fig. 2(c). These curves terminate abruptly close to the light line, because CPPs become ill-defined once they couple to either radiation modes or SPPs, due to radiation losses. For reference Fig. 2(c) shows the light cone (discontinuous black curve) and the dispersion relation of SPPs of the flat surface (contin-

#132559 - $15.00 USD Received 2 Aug 2010; revised 9 Sep 2010; accepted 10 Sep 2010; published 27 Oct 2010

uous black curve). The relation between CPPs and TWG modes is clear. For large k_z, CPPs are strongly confined at the apex of the channel, and their dispersion relation virtually coincides with those for T_{1o} and T_{2o} modes. As k_z gets smaller, approaching the light cone, the field gets less localized and "feels" whether the top surface is open (as in channel waveguides) or close (as in a TWG). Correspondingly, the dispersion relation of CPPs and TWG modes deviate close to the light line. Still, as Fig. 2(c) shows, the field for modes with odd parity is fairly localized at the apex of the α-angle (which is the most acute in the triangle considered), even at cutoff. As previously discussed, each β-angle of the TGW can also support confined modes but, first, as these angles are wider the modes would be less localized, and second, in an isosceles triangle with two β angles these electromagnetic modes hybridize.

Transmission resonances based on these strongly localized modes depend weakly on angle of incidence. The experimental transmission versus both frequency and parallel momentum of the incident light are shown in Fig. 3, for different orientations of the electric field and tilt angles. The corresponding computed band structure of leaky EM modes in the considered array of triangular holes are depicted with circular symbols. For reference, the figures also show the dispersion relation of the SPPs of a flat silver surface (continuous grey line) and the relation between parallel momentum and wavelength for incident radiation $k_x = 2\pi P \sin\theta/\lambda$, for two angles of incidence $\theta = 22^o$ and $\theta = 45^o$ (oblique dashed lines). There is a close correspondence between experimental and computed resonances. Notice, however, that the computed resonances are ~ 0.2 eV lower than the experimental ones which is due to the sharpness of the triangular corners considered in the calculations. Also, some modes appearing in the computed band structure do not show up in the experimental transmission data because, as Fig. 2 revealed, they should appear in the absorption and reflection spectra. In any case, the experimental data clearly show that several modes present a very small dispersion over the available tilt angles. This is corroborated by the calculations, which further demonstrate that the property of very weak dispersion extends over the whole Brillouin zone, at tilt angles larger than those accessible in the experimental setup.

3. Conclusion

We have shown that triangular holes having a small acute angle and sizes of a few hundreds of nanometers, present cutoff wavelengths that are much larger than what could be expected from their size. The physical mechanism is the existence of "channel-plasmon-like" modes, mainly confined at the acutest angle of the triangular waveguide. This phenomenon should thus occur for any hole shape with acute angles (and sustaining sides sufficiently long). An array of such holes presents EOT due to these localized cavity modes, which appear close to the cutoff condition. Due to the strongly confined nature of the electromagnetic field in the hole, these modes show little angular dispersion. This makes triangular holes with very acute angles excellent candidates for EOT applications that require insensitivity and/or integration over a broad range of angles of incidence.

Acknowledgments

The authors acknowledge support from the STREP "Plasmon Enhanced Photonics" (IST-FP6-034506), the Spanish Ministry of Science and Innovation (grants MAT2008-06609-C02 and CSD2007-046-NanoLight.es), and from the ERC (grant 227577).

#132559 - $15.00 USD Received 2 Aug 2010; revised 9 Sep 2010; accepted 10 Sep 2010; published 27 Oct 2010